Modelling of Multiphase Flow in Ironmaking Blast Furnace

ARTICLE *in* INDUSTRIAL & ENGINEERING CHEMISTRY RESEARCH · JUNE 2008

Impact Factor: 2.59 · DOI: 10.1021/ie800147v

Modelling of Multiphase Flow in Ironmaking Blast Furnace

X. F. Dong, A. B. Yu,*, and J. M. Burgess

Laboratory for Simulation and Modelling of Particulate Systems, School of Materials Science and Engineering, The University of New South Wales, Sydney, NSW 2052, Australia

D. Pinson, S. Chew, and P. Zulli

Bluescope Steel Research, P.O. Box 202, Port Kembla, NSW 2505, Australia

A mathematical model for the four-phase (gas, powder, liquid, and solids) flow in a two-dimensional ironmaking blast furnace is presented by extending the existing two-fluid flow models. The model describes the motion of gas, solid, and powder phases, based on the continuum approach, and implements the so-called force balance model for the flow of liquids, such as metal and slag in a blast furnace. The model results demonstrate a solid stagnant zone and dense powder hold-up region, as well as a dense liquid flow region that exists in the lower part of a blast furnace, which are consistent with the experimental observations reported in the literature. The simulation is extended to investigate the effects of packing properties and operational conditions on the flow and the volume fraction distribution of each phase in a blast furnace. It is found that solid movement has a significant effect on powder holdup distribution. Small solid particles and low porosity distribution are predicted to affect the fluid flow considerably, and this can cause deterioration in bed permeability. The dynamic powder holdup in a furnace increases significantly with the increase of powder diameter. The findings should be useful to better understand and control blast furnace operations.

1. Introduction

An ironmaking blast furnace (BF) is a complex reactor that involves counter-current, co-current, and/or cross-current flows of the gas, powder, liquid, and solids phases. As shown in Figure 1, in this process, iron-bearing materials and coke are charged at the top of the BF and hot air (blast) enters the furnace through the tuyeres in the lower part and combusts carbonaceous materials (coal, coke), to produce a reducing gas. As the reducing gas ascends, it reduces and melts the iron-bearing materials to form liquid iron and slag in the cohesive zone (CZ). These liquids percolate through the lower zone coke bed to the hearth. If pulverized coal injection (PCI) is practiced and at high rates, unburnt coal may leave the raceway region entrained in the gas.[1] Under some conditions, the holdup of the fines results in deterioration of furnace permeability. Understanding the behavior of this multiphase flow system is very important for process control. Because of the difficulty of in situ sampling and measurement in the BF, numerical modeling and simulation, often coupled with physical modeling, has had an important role in achieving this goal.[2,3]

Various models have been developed previously to numerically investigate gas−solid, gas−liquid, and gas-powder flows in packed beds, as briefly described in the following. Typically, two approaches have been used to model solid flow: discrete and continuum.[4–11] The discrete approach is based on the analysis of the motion of individual particles and has the advantage that there is no need for global assumptions on the solids, such as steady-state behavior or uniform constituency, and/or constitutive relations. However, this approach is still not suitable for simulation of large-scale reactors such as a BF that contains a very large number of particles, because of the current limited computational capacity. Instead, the continuum approach, which treats the solid particles as a continuous phase, is widely applied to predict the flow of solids, including velocity distribution and flow zones. In particular, one solution procedure has also been proposed to calculate the profile of the stagnant zone.[10] Knowledge of the burden distribution and velocity field makes it possible to compute the flow fields of other phases.

Liquid flow in the BF has several interesting features that distinguish it from other gas−liquid co-current and counter-current flows in the chemical and manufacturing industries. These include the nonwetting between liquids and coke particles,

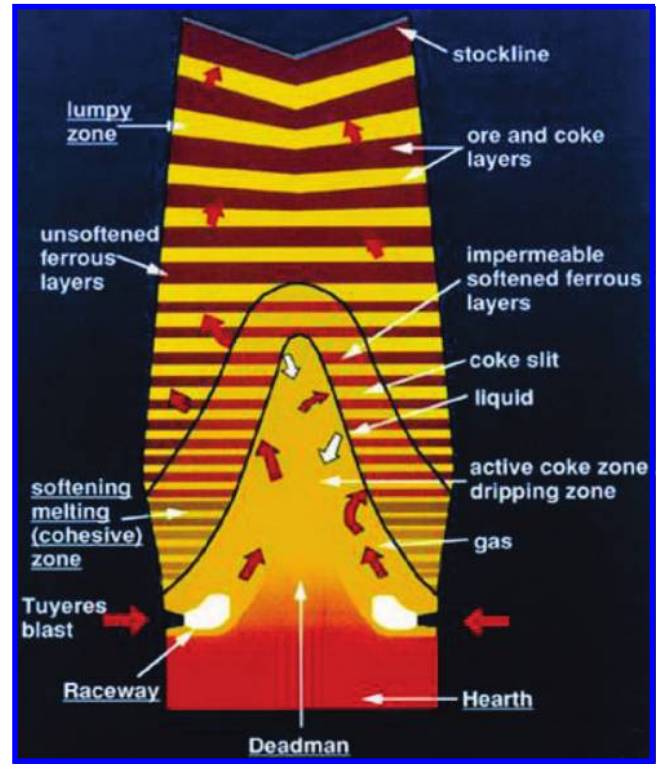

Figure 1. Schematic illustration of internal flow phenomena in a blast furnace (BF).

* To whom correspondence should be addressed. Tel.: 61 2 93854429. Fax: 61 2 93855956. E-mail address: a.yu@unsw.edu.au.

10.1021/ie800147v CCC: $40.75
Published on Web 06/27/2008

Table 1. The Meaning of τ and Source Terms Presented in eq 1

equation name	i	Ψ_i	τ_i	S_{ψ_i}
gas continuity	g	1	1	0
gas momentum	g	$\mathbf{u}_g$	$\varepsilon_g\mu_g[\nabla\mathbf{u}_g + (\nabla\mathbf{u}_g)^T] - {}^2/_3\varepsilon_g\mu_g(\nabla\cdot\mathbf{u}_g)\mathbf{I}$	$-\varepsilon_g\nabla p + \rho_g\varepsilon_g\mathbf{g} + \mathbf{F}_g^s + \mathbf{F}_g^f + \mathbf{F}_g^l$
powder continuity	fd	1	1	S_f
powder momentum	fd	$\mathbf{u}_f$	$\varepsilon_{fd}\mu_f[\nabla\mathbf{u}_f + (\nabla\mathbf{u}_f)^T] - {}^2/_3\varepsilon_{fd}\mu_f(\nabla\cdot\mathbf{u}_f)\mathbf{I}$	$-\varepsilon_{fd}\nabla p - p_f + \rho_f\varepsilon_f\mathbf{g} + \mathbf{F}_f^s + \mathbf{F}_f^g + \mathbf{F}_f^l$
solid continuity	s	1	1	S_s
solid momentum	s	$\mathbf{u}_s$	$\varepsilon_s\mu_s[\nabla\mathbf{u}_s + (\nabla\mathbf{u}_s)^T] - {}^2/_3\varepsilon_s\mu_s(\nabla\cdot\mathbf{u}_s)\mathbf{I}$	$-\varepsilon_s\nabla p_s + \rho_s\varepsilon_s\mathbf{g}$

coexisting immiscible slag and iron liquid phases, low liquid holdup, and slow discrete liquid flow. Because of the interaction with the gas phase, some special phenomena may also be present for the liquids, such as flooding and the existence of a "dry" zone in the furnace. In the past, different models have been proposed to describe the gas and liquid flow in the BF, including potential flow model,[12–14] probability model,[15] probability−continuous model,[16] tube network dynamic model,[17] and force balance model.[18–21] Among these models, the force balance model is perhaps the most attractive, because of its advantages in computation and representation of the relevant physics of liquid flows through a packed bed (see, for example, Wang et al.[19,22] Coupled with the stochastic model, liquid spreading in a packed bed can also be taken into account.[19] Recently, Chew et al.[21] implemented an online modeling tool to simulate the conditions in an industrial BF, and this gave a reasonable prediction for global hydrodynamic quantities such as liquid holdup and pressure drop.

Recently, attempts have also been proposed[2,23–34] to model the gas and powder flow in a packed bed, where the powder phase is either tracked as individual particles, powder clusters[33,34] or treated as a continuous medium with properties analogous to those of a fluid. Application of the former treatment is much limited by the computational competency. The latter treatment is commonly accepted in laboratory- and industry-scale simulations, although there are different simplifications and/or assumptions in the numerical models used. Attempts have been made to apply the continuum approach to gas−powder flow in both simple and complex situations, with regard to the following three aspects: (i) quantification of the relationship between pressure loss, powder holdup, and powder/gas feed rate;[2,23,24,26,27,30] (ii) prediction of powder accumulation phenomena;[23,25,28,29,31] and (iii) simulation of the BF process.[26,28,29,32,35]

Previous studies clearly demonstrated that numerical simulation of two-phase flow in packed beds is possible. Recently, attempts have also been made to model multiphase flow.[14,36–38] However, these attempts require simplifications for (a) the internal structure of the BF (e.g., the layered structure of CZ is not fully considered); (b) fluid flow when four phases are simultaneously considered, especially for powder and liquid phases; and (c) interphase coupling (e.g., interaction force between powder and liquid). The simplifications, in particular nonlayered CZ treatment, make the prediction of multiphase flow in the lower part of the BF unrealistic.

In this paper, a mathematical model has been proposed to describe the gas−powder−liquid−solid four-phase flow in a blast furnace to overcome the deficiency identified above. The model is developed by extending the existing two-phase flow models for gas−solid, gas−liquid, and gas−powder flows. The characteristics of gas−powder−liquid multiphase flow in moving particles under BF conditions are studied on this basis. The work provides a sound basis to predict the multiphase flow, phase holdup distribution and, after coupling with heat transfer and chemical reactions, the performance of BFs.

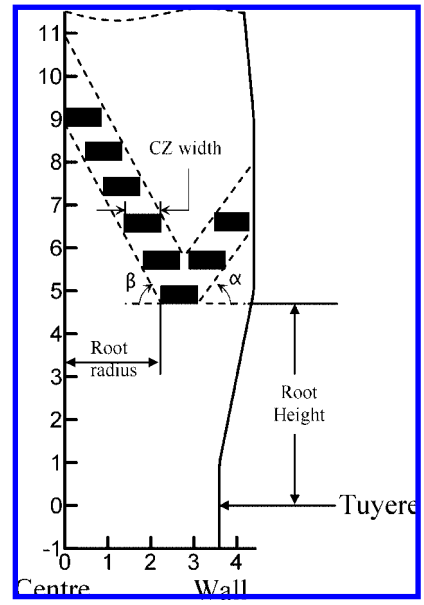

Figure 2. Definition of the CZ parameters (values shown in meters).

2. Numerical Modeling

2.1. Governing Equations. The present modeling treats gas, solid, and fine powders as continuous phases. The so-called "viscous model"[9] is used for the solid phase, in which the stagnant region is predicted by the method proposed by Zhang et al.[10] Correspondingly, the two-fluid model is extended to simulate the gas−powder flow, and a new procedure is used to address the possible powder accumulation in the furnace hearth.[31] Therefore, the equations governing the flow of gas, solids, and powders are written as

$$\nabla\cdot(\varepsilon_i\rho_i\mathbf{u}_i\Psi_i) = \nabla\cdot\tau_i + S_{\Psi_i} \quad (1)$$

where Ψ represents the conserved quantity (see Table 1). The stress tensor τ_i is given in Table 1, together with a source term S_{ψ_i}, which contains pressure, interaction force, gravity force, and other terms not listed in eq 1. (Note that a presumed powder−liquid interaction force is used in the sensitivity tests presented in Section 4.4.) In the aforementioned equations, the consumption of solids (S_s) in the lower part of a BF takes into account the shrinkage and meltdown of ore, and the gasification, carburization, and combustion of coke. The consumption of pulverized coal occurs via the solution loss reaction, direct reduction in the stack, carburization in the bosh, and combustion in the raceway.

A force balance model[20] is used to calculate the liquid flow, in which the liquid (metal or slag) in a BF is treated as discrete droplets or rivulets, quickly achieving a steady average percolation velocity based on gas, liquid, and packing properties. The behavior of liquid droplets is governed mainly by three forces: the gas drag force F_{ld}^g, the bed resistance force F_{ld}^s, and gravity force $F_{ld}^{gravity}$. Note that, for simplicity, the interaction force between powder and liquid is ignored here. According to the force balance, the sum of the three forces is macroscopically equal to zero for the liquid flow at the steady state:

$$\mathbf{F}_{ld}^g + \mathbf{F}_{ld}^s + \rho_l\mathbf{g}h_{ld} = 0 \quad (2)$$

In the entire system, the total volume fraction occupied by the phases is expressed as

$$\varepsilon_g + \varepsilon_s + \varepsilon_{fd} + \varepsilon_{fs} + h_{ld} + h_{ls} = 1 \quad (3)$$

Table 2. Empirical Correlations for the Interaction Forces between Phases

phase	interaction forces	references
gas−solid, G−S	$\mathbf{F}_g^s = -\mathbf{F}_s^g = -\left[150\frac{(\varepsilon_s+\varepsilon_{fs})^2}{\varepsilon_g+\varepsilon_{fd}}\frac{\mu_g}{(\varphi_s d_s)^2} + 1.75(\varepsilon_s+\varepsilon_{fs})\frac{\rho_g}{\varphi_s d_s}\lvert\mathbf{u}_g - \mathbf{u}_s\rvert\right](\mathbf{u}_g-\mathbf{u}_s)$	25, 31
gas−liquid, G−L	$\mathbf{F}_g^{ld} = -\mathbf{F}_{ld}^g = -\left(\frac{h_{ld}}{d_l}+\frac{A_{sld}}{6}\right)\left[150\left(\frac{\varepsilon_s+\varepsilon_{lt}}{d_w}\right)\mu_g + 1.75\rho_g\lvert\mathbf{U}_g\rvert\right]\frac{\mathbf{U}_g}{\varepsilon_g^3}$	20
	where $d_l = \max\{d_{lg}, d_{lh}\}$	
	$d_{lg} = \frac{\max\{-6.828\ \mathrm{sign}(\sqrt{X_p}-0.891)(\sqrt{X_p}-0.891)^2, 0\} + 0.695}{\sqrt{\rho_l g/\sigma}}$	
	$d_{lh} = \frac{\max\{6.828\ \mathrm{sign}(f_6)(f_6)^2, 0\} + 0.695}{\sqrt{\rho_l g/\sigma}}$	
	$f_6 = \left(\frac{\max\{\ln(h_{lt}/h_{lto}), 0\}}{0.513}\right)^{(1/2.642)} - 0.891$	
	$X_p = \frac{\Delta P_e}{\Delta x \rho_l g}\left\{\frac{\rho_l g \varphi^2 d_g^2}{\sigma \varepsilon_s^2}\right\}^{0.3}(1+\cos\theta)^{-0.5}$	
gas−fine powder, G−F	$\mathbf{F}_g^f = -\mathbf{F}_f^g = -\frac{3}{4}C_d\frac{\varepsilon_g\rho_g\varepsilon_{fd}}{\varphi_f d_f}\lvert\mathbf{u}_g-\mathbf{u}_f\rvert\varepsilon_g^{-2.65}(\mathbf{u}_g-\mathbf{u}_f)$	24, 39
	where $C_d = \begin{cases}\frac{24}{Re} & (\text{for } Re_f \le 1)\\ \frac{24}{Re_f}(1+0.15Re_f^{0.687}) & (\text{for } 1 < Re_f \le 1000)\\ 0.44 & (\text{for } 1000 < Re_f)\end{cases}$	
fine powder−solid, F−S	$\mathbf{F}_f^s = -\frac{1}{2D^*}\rho_f\varepsilon_{fd}\lvert\mathbf{u}_f-\mathbf{u}_s\rvert f_k(\mathbf{u}_f-\mathbf{u}_s)$	24
	where $f_k = 14.98/Fr_f^{1.33}$ (for $0.03 < Fr_f < 0.5$)	
liquid−solid, L−S	$\mathbf{F}_{ld}^s = \left(\frac{150}{36}\mu_l\frac{A_{sld}^2}{h_{ld}^3}+\frac{1.75}{6}\rho_l\frac{A_{sld}}{h_{ld}^3}\lvert\mathbf{U}_l\rvert\right)\mathbf{U}_l$	20

In eq 3, ε_{fs} and h_{ls} can be calculated using the empirical equations given in the next section.

The significant parameters that characterize the behavior of the multiphase system are the interaction forces between the gas, powder, and particle phases, as summarized in Table 2.

2.2. Boundary Conditions and Numerical Solution. Four sets of conservation equations, closed by the constitutive equations and supplemented with the boundary conditions, are solved numerically. A no-slip boundary condition for the gas phase and a full-slip boundary condition for the solid phase are applied in this work. For the powder phase, a partial slip boundary condition is assumed, so that the powder tangential velocity at the wall is assumed to be proportional to its gradient at the wall:[40]

$$u_{fw} = -\lambda_f\frac{\partial u_f}{\partial x}_w \tag{4}$$

where the x-direction is normal to the wall. The slip parameter λ_f is the mean distance between particles, and it can be estimated using the relation

$$\lambda_f = \left(\frac{1}{\varepsilon_f^{1/3}}\right)d_f \tag{5}$$

Equation 5 implies that, for small particles, the boundary condition is close to the no-slip condition. At the inlet, Dirichlet boundary conditions are specified for the gas, powder, and liquid phases; at the outlet, Neumann boundary conditions are applied (i.e., the variable gradient is zero). In this work, only the slag

Table 3. Blast Furnace Simulation Conditions

variable	value
gas density	1.25 kg/m^3
gas viscosity	1.8×10^{-4} kg m^{-1} s^{-1}
superficial gas velocity	1.00 m/s
powder diameter	75 μm
powder density	1400 kg/m^3
powder mass flux	0.154 kg m^{-2} s^{-1}
solid density of mixture	2200 kg/m^3
solid charging rate	5000 t/day
slag density	2600 kg/m^3
slag viscosity	1.0 kg m^{-1} s^{-1}
surface tension	0.47 N/m
contact angle	90°
particle shape factor	0.8
productivity	2000 t/day
slag rate	380 kg/t
cohesive zone shape	W

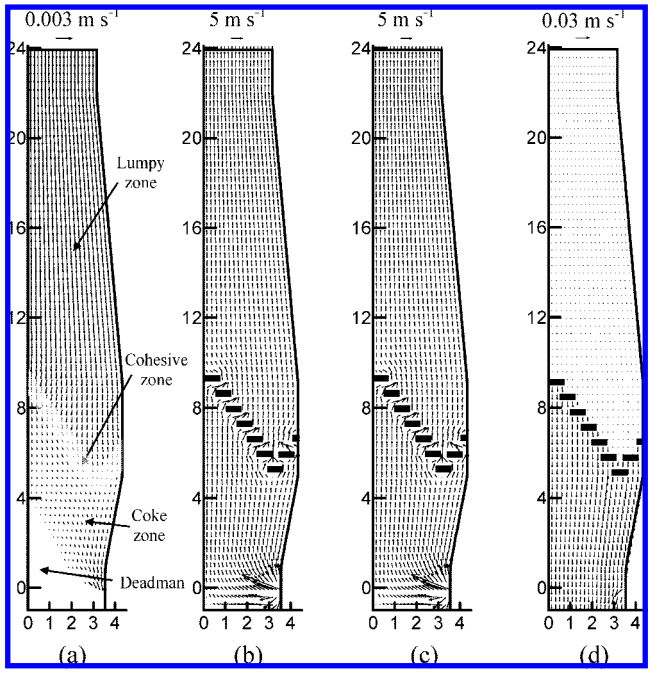

Figure 3. Velocity vectors distribution in a BF with a W-shaped CZ: (a) solid flow, (b) gas flow, (c) powder flow, and (d) liquid flow.

phase is considered. This liquid phase is assumed to be generated from the bottom of each fused layer in the CZ, and inlet velocity and volume fraction are specified based on the given slag mass flow rate calculated from the total productivity of the BF.

The present work is focused on flow modeling and does not consider heat and mass transfer. To be effective, therefore, the shape of CZ is specified. The solid flow field is calculated with the use of this information, from which the deadman boundary is determined via a solid isovelocity curve.[10] With the layered ore and coke in the BF modeled as a homogeneous mixture, the assumption is made that solid iron ore is completely consumed (transformed to molten liquid) in the CZ. Coke flows toward the raceway, where it is consumed by reacting with oxygen in the blast. It is also consumed in other zones of the furnace by, e.g. carbon dissolution in liquid metal in the coke zone, deadman, and hearth. The solid consumption rate S_s (kg m^{-3} s^{-1}) varies in a BF and, following the work of Zhang et al.,[41] is determined as follows. Above the CZ, the consumption is negligible; in the CZ, iron ore is fully consumed as a result of softening and melting, i.e., $S_s = (S_{flowrate} \times OSM)/(TCO \times VOL_{cz})$; and below the CZ, the coke consumption is given as $S_s = (S_{flowrate} \times CSO)/(TCO \times VOL_{bcz})$ to represent the coke

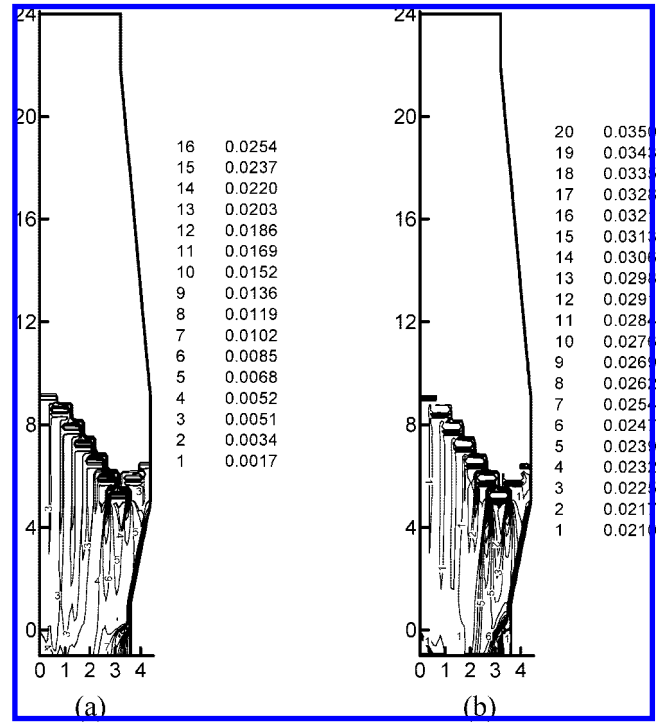

Figure 4. Calculated liquid holdups in a BF with a W-shaped CZ: (a) dynamic holdup and (b) total holdup.

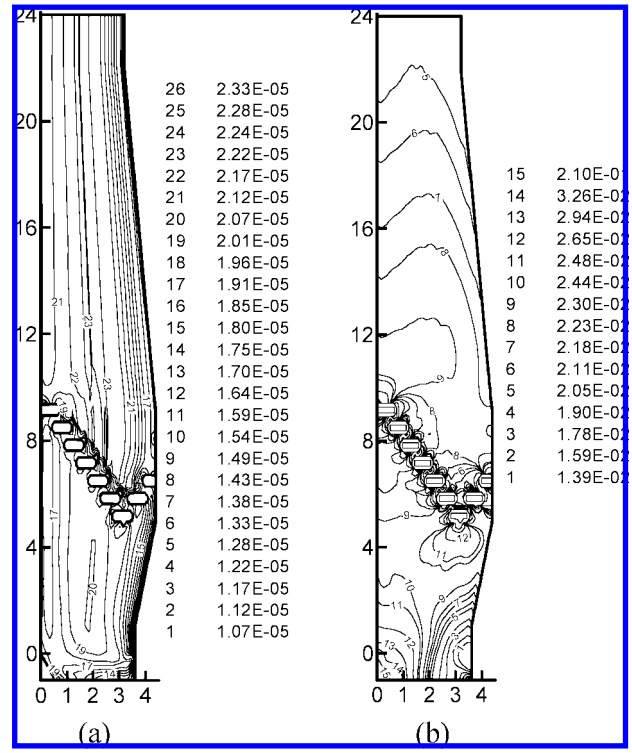

Figure 5. Calculated powder holdups for the W-shaped CZ: (a) dynamic holdup and (b) total holdup.

solution loss. Unburnt char leaving the raceway may also be consumed in the furnace, which can be calculated using the equation

$$S_f = S_{hotmetal} \times \frac{CCR}{VOL_{zone}}$$

Some char will be entrapped by packed coke particles, or accumulate in the furnace hearth and CZ. The remaining fine

Table 4. Region Properties

property	Value		
	case 1	case 2	case 3
	Lumpy Zone		
d_s	0.04 m	0.04 m	0.04 m
ϵ	0.4	0.4	0.4
CCR	0	0	8.1
	Cohesive Zone		
d_s	0.035 m	0.035 m	0.035 m
ϵ	0.4	0.36	0.36
CCR	0	0	0
	Coke Zone		
d_s	0.03 m	0.03 m	0.03 m
ϵ	0.4	0.4	0.4
CCR	0	0	24.3
	Deadman		
d_s	0.02 m	0.02 m	0.02 m
ϵ	0.4	0.35	0.35
CCR	0	0	8.1
η_{pc}[a]	0%	0%	84%

[a] The symbol η_{pc} represents the pulverized coal combustion rate in the raceway.

char will escape with the off-gas from the top of the furnace. In this work, the static holdup for a fixed bed is quantified by the equation (modified from that of Hidaka et al.[27])

$$\varepsilon_{fs} = \min\{c_1 U_g^{n_1} G_f^{n_2}, \varepsilon_f^{max}\} \quad (6)$$

for the system, where $d_f = 75\ \mu$m, $c_1 = 0.018$, $n_1 = -0.75$, and $n_2 = 0.2$. The term ε_f^{max} corresponds to the situation when the voids among packed particles are fully occupied by powder.[42] The region with this maximum powder holdup, which is referred to as the powder accumulation region, will not allow any powder to penetrate, thus providing a boundary to powder flow. The technique used to calculate the gas−powder flow and powder accumulation region has been reported elsewhere.[31]

Because there is a significant difference between static holdups in fixed and moving beds,[43] the powder holdup correlations for gas−powder two-phase flow in a fixed bed cannot be directly used to describe the behavior of gas−powder flow in moving beds. A new correlation for static holdup with the effect of packed particle movement is expressed as the ratio of the static holdups between moving and fixed beds:

$$\frac{\varepsilon_{fs\text{-}M}}{\varepsilon_{fs\text{-}F}} = \exp\left(-2.765\times 10^5 Re_g^{-1.6} Fr_s^{1.04}\right) \quad (7)$$

where $Re_g \in (40, 200)$, and $Fr_s \in (0, 0.004)$. This equation can be used to extend the existing correlations for use in applications other than fixed beds (i.e., in the present BF study with PCI operation).

Static liquid holdup can be calculated using the following modified equation, in which the gas effect is considered:[20]

$$h_{ls} = (21.0 + 0.305 Cp_m)^{-1} \exp[0.513\ \mathrm{sign}(X_p)|X_p|^{1.321}] \quad (8)$$

The main procedures used for the calculation of four-phase flow are described as follows:

(1) Calculate solid flow field under the boundary conditions and relevant consumption rates;[9,10]

(2) Determine the gas-powder flow field using the solid flow field;[30,31]

(3) Guess the liquid−solid contact area A_{sld}^*;

(4) Solve the force balance equations combined with the correlations[20] to obtain the liquid holdup (h_{lt});

(5) Calculate the liquid holdup ($h_{lt,continuity}$) by mass continuity;

(6) Treat the updated area term $A_{sld} = A_{sld}^*[(1 - \alpha_l) + \alpha_l h_{lt}/h_{lt,continuity}]$ as a new guess for A_{sld}^*, return to step 4, and repeat the entire procedure until a converged solution for liquid flow field is obtained;

(7) Repeat steps 1−6 until convergence.

3. Model Validation and Simulation Conditions

The formulation of the current four-phase flow model is actually a combination of the previously mentioned two-fluid models.[10,19–21,31] These two-fluid models and their corresponding numerical algorithms have been verified in the study of gas−solid,[10,41] gas−powder,[31,35] and gas−liquid flows,[19–22] respectively. On this basis, the present four-phase flow model is directly used to assess the BF flow. Its validity will be discussed in relation to the predictions against the common understanding of the flow phenomena in a BF.

As listed in Table 3, numerical simulations have been performed in two dimensions under conditions similar to that of a BF with an inner volume of 1000 m^3 (hearth diameter = 7.2 m, height = 25 m) with a productivity of 2000 tonnes of hot metal (tHM) per day and a slag rate of 380 kg per tHM. The computational domain is composed of 148 × 38 body-fitted control volumes, in a two-dimensional axisymmetric grid that represents the BF region from just above the burden surface to above the surface of the slag in the hearth. Various operational conditions, including different inlet gas flow rates, powder diameters, and solid charging rates, are applied in this study to investigate their effects on fluid flow. A CZ is modeled by inserting solid blocks in the bed to represent the fused ore layers (equal thicknesses of the ore and coke layers are assumed). In practice, the CZ layers are relatively impermeable to gas and powder flow,[44] and, here, they are modeled by a series of dummy cells in the simulation. For the solid flow, ore is assumed to be completely consumed in the CZ region and coke flows through the CZ. For the liquid phase, the bottom of each layer in the CZ is the liquid inlet to the BF lower zone.

In this study, the CZ is characterized by several parameters, as shown in Figure 2. These include the root radius (2.75 m) and height (5.1 m), the width of the CZ (0.6 m), and the incline angles ($\alpha = 55°$, $\beta = 55°$).

4. Results and Discussion

4.1. General Flow Fields. Figure 3a shows the calculated results for solid flow with a W-shaped CZ. With a homogeneous mixed burden downward flow, the ore is softened, fused, and eventually melted in the CZ. In the upper section of a BF, the solid velocity decreases with the descent as a result of the expanding cross-sectional area. The flow in this portion of the BF is plug flow. When the mixed burden passes through the cohesive zone, the velocity decreases because the solid ore is completely transformed to liquid; here, ore is assumed to be uniformly consumed in the CZ region. Coke then flows toward the raceway, with some mass loss, because of carburization in the coke zone. In the deadman, the flow of coke is quasi-discontinuous and, as such, the residence time of coke in the deadman is long. In this lower zone, the solid flow converges due to the converging walls and the existence of the deadman. Through the results shown in Figure 2a, four regions in the BF can be identified: the lumpy zone, the cohesive zone, the coke zone, and the deadman. These flow patterns (and zones) have been observed in the previously reported experiments.[8]

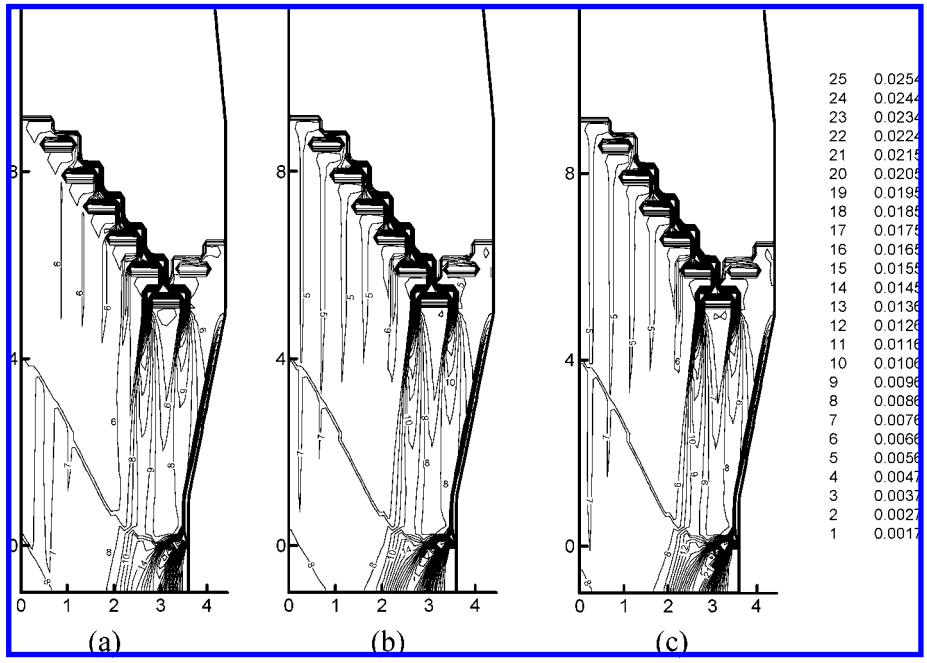

Figure 6. Dynamic liquid holdup distribution in the BF modelled: (a) case 1, (b) case 2, and (c) case 3. (Values shown are given in units of m^3/m^3.)

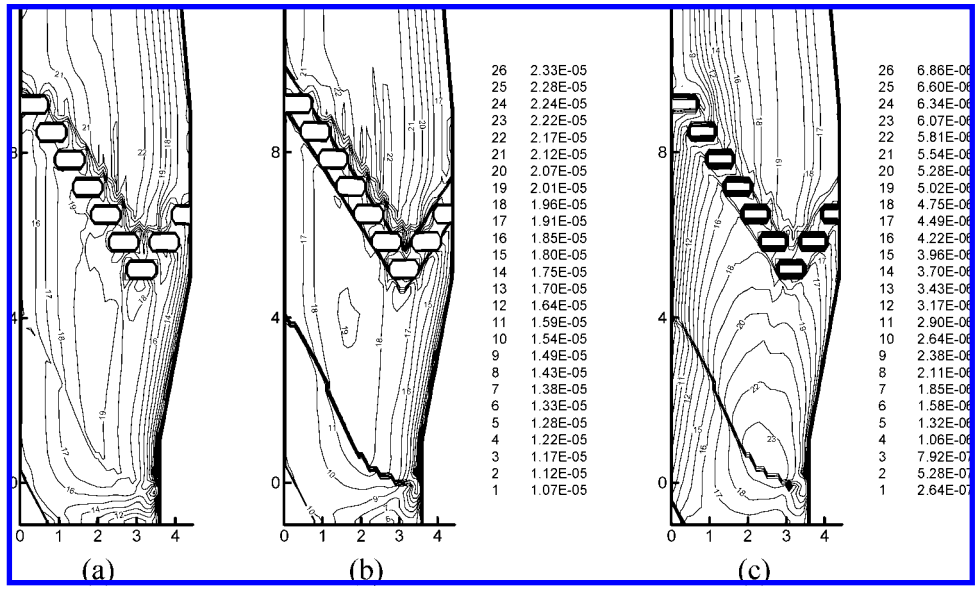

Figure 7. Dynamic powder holdup distribution in the BF modelled: (a) case 1, (b) case 2, and (c) case 3. (Values shown are given in units of m^3/m^3.)

Figures 2b and 2c demonstrate that the coke layers in a W-shaped CZ act as a gas and powder distributor, giving different flow trends below and above the CZ. Near the corner of the upper surfaces of the CZ layers, converging flow leads to the formation of a low gas and powder velocity region. However, a strong horizontal gas−powder flow can form in the coke slits within the CZ layers. There is a low gas and powder flow region in the lower central region of the BF. A comparison of the velocity vectors for the gas and powder phases shows that powder does not follow the gas flow exactly, because of their differences in density, viscosity, and interaction with packed particles. Figure 3d shows that liquid slag generated in the layered CZ can flow downward through the coke zone to the hearth with a nonuniform liquid flow distribution. In particular, at the sides of the lowest part of the CZ, the liquid velocity is relatively large, which indicates that an active liquid flow zone exists there. Near the raceway, the liquid flow strongly deviates from the vertical direction, because of the effect of horizontal gas flow.

Figure 4 shows the calculated liquid holdup distribution in the furnace, given a particle diameter of 0.04 m and bed voidage of 0.4. Maldistribution of dynamic and total liquid holdup is significant throughout the lower portion of the furnace, noting that the total holdup is equal to the sum of the dynamic and static holdups. The results demonstrate that the liquid generated in one layer can accumulate and then spread on top of the next fused layer. A fraction of the liquid flows inward and combines with the liquid source generated at this fused layer to form the relative dense liquid flow channel, generating a so-called "icicle".[19,22] The remaining fraction of liquid flows outward, along the cohesive layers. Note that liquid flow outward along the cohesive zone may induce the liquid solidification in the low-temperature environment. However, because only impermeable layers in the cohesive zone and fluid flow are considered

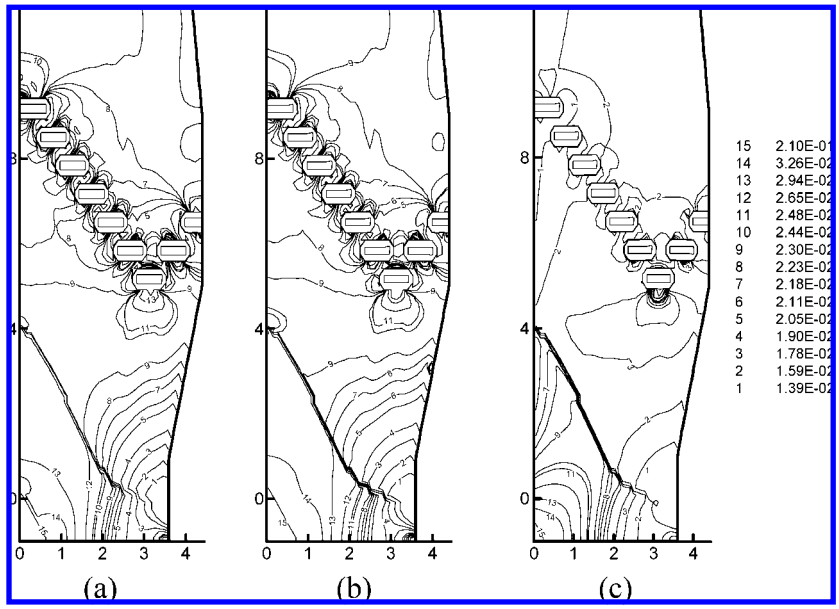

Figure 8. Total powder holdup distribution in the BF modelled: (a) case 1, (b) case 2, and (c) case 3. (Values shown are given in units of m^3/m^3.)

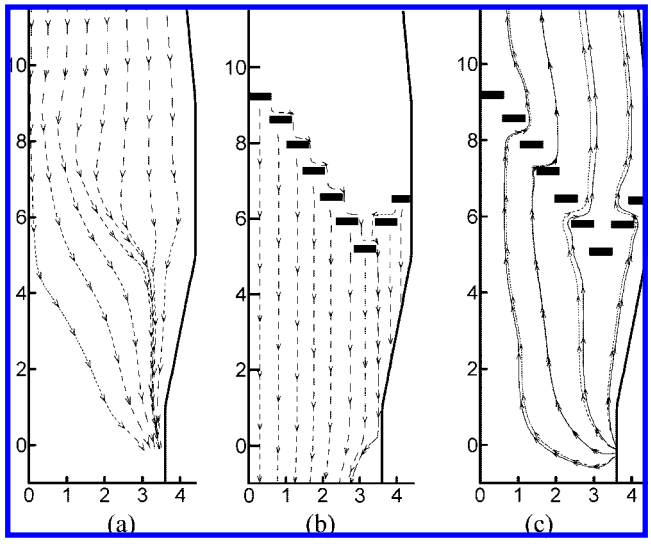

Figure 9. Streamlines of (a) solid, (b) liquid, and (c) gas−powder flow in the BF modelled. Note that the solid line in panel c represents the gas streamline.

in this study, this situation cannot be simulated. The predicted liquid flow field implies that, in reality, it is inevitable for liquid phase to flow in a relatively low-temperature region in and around the cohesive zone. This result is consistent with the experimental observation.[45] The combination of liquid sources at every layer and liquid streams flowing downward from the top creates a significant liquid stream at the lowest part of the CZ. This stream flows down along the two sides of a layer through the coke zone and, hence, can strongly interact with the gas flow in front of the tuyere.

Figure 5 shows the calculated dynamic and total powder holdups as volume fraction contours. Below the CZs, the maximum dynamic holdup can be observed in the mid-radius region. Above the CZ, the W-shaped CZ generates a plume-shaped dynamic powder hold-up distribution. The contours of dynamic holdup seem to extend from the individual cohesive layers. "Plumes" of dynamic holdup are located at the intersection of the streamlines of the powder flow with the layers. The stratified distribution of dynamic holdup may result in a nonuniform distribution of process variables, such as temperature and gas composition.

The calculated total powder holdup distribution is shown in Figure 5b, where a powder accumulation region can be identified in the lower portion of the BF. As can be seen, a relatively dense powder distribution occurs immediately below the lowest portion of the CZ. Generally, powder is likely to accumulate in the low-gas-flow region, as previously described.[26] The total powder holdup gradually increases from the inlet to the accumulation region. Also, the magnitude of liquid holdup increases in the central dense powder holdup region (powder accumulation region). This indicates that once powder accumulation occurs, permeability can be further reduced by the liquid phase. In the CZ, the increased gas velocity induces low powder holdup in the coke slits between the impermeable fused ore layers. However, at the corner of some layers, there are dense powder holdups. Because of the movement of solids, the powder distribution in the coke zone is relatively loose. As solid particles move downward, the deposited powder will discharge with the solid particles, and contact points between solid particles will continuously change, so that powder has a lesser chance to deposit in the contact region of solid particles. This implies that, in the furnace, the deadman may have the worst permeability, because of very low solids velocity. Interestingly, because of the existence of a liquid phase in the lower portion of the furnace, gas velocity increases correspondingly with the reduced available pore volume, which induces a lower powder holdup, compared to that above the CZ, where porosity is large but without the liquid phase present.

4.2. Effect of Local Packing Properties. The simulation in section 4.1 is limited to a furnace of uniform bed properties. A real BF is often nonuniform, in regard to packing structure. It is important to understand the effect of such nonuniformity on fluid flow. This can be obtained through the incorporation of local properties into the model previously developed. As part of this work, simulations have been conducted to examine this nonuniform behavior. Table 4 lists conditions for different regions in the present simulation of the four-phase flow, which were designed to investigate the effect of continuously decreasing the particle size from the cohesive zone to the deadman

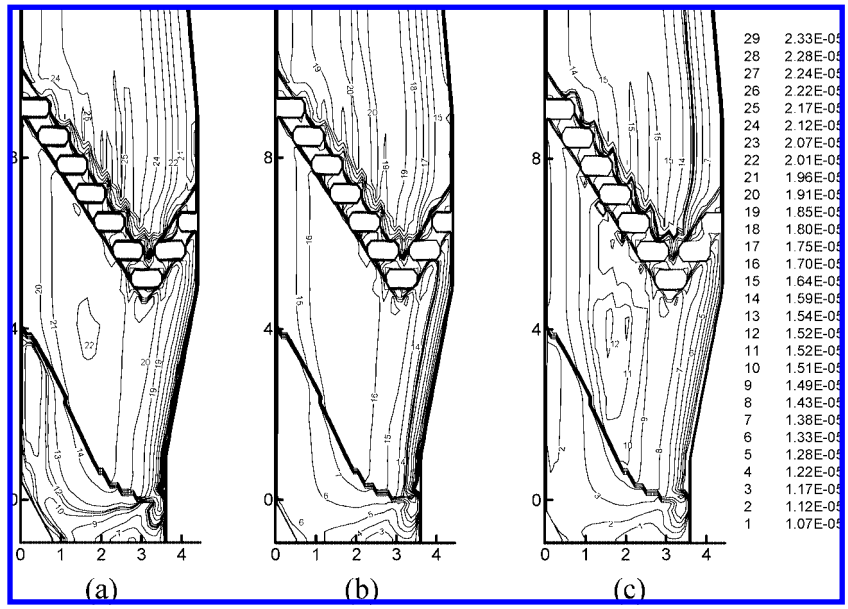

Figure 10. Dynamic holdup distribution for different superficial gas velocities: (a) 1.00 m/s, (b) 1.12 m/s, and (c) 1.27 m/s.

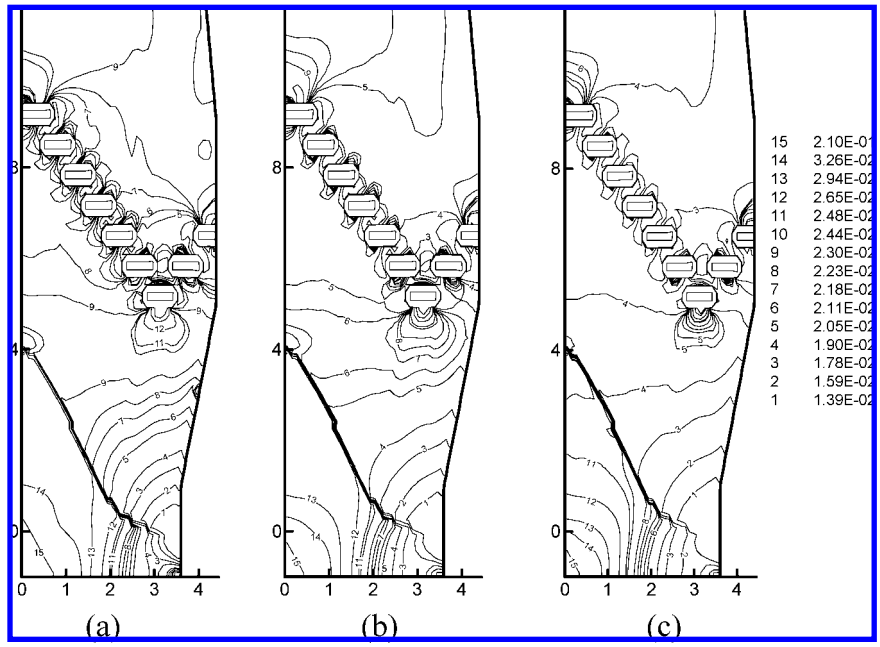

Figure 11. Total holdup distribution for different superficial gas velocities: (a) 1.00 m/s, (b) 1.12 m/s, and (c) 1.27 m/s.

(case 1), lower permeability cohesive zone and deadman (case 2), and powder possible consumption in BF (case 3) on the fluid flow.

Figure 6 shows the effects of variations in local mean particle size, regional porosity, and powder consumption rates on dynamic liquid holdup, corresponding to cases 1−3 in Table 4. As the particle size in the deadman deceases, dynamic holdup is likely to increase, in comparison to Figure 4a. In the coke zone between the deadman and CZ, the liquid flow distribution is similar to that previously shown, except that the icicles have been shortened and some reorganization has occurred. A higher level of holdup at the surface of the deadman is observed with a reduction in the particle size. In the upper part, the flooding contour of dynamic holdup shows that liquid holdup increases as the liquid flows down along the cohesive layer. In the lower part, the liquid holdup is high in the corner of the deadman and in front of the dry zone. Similarly, when the porosity in the

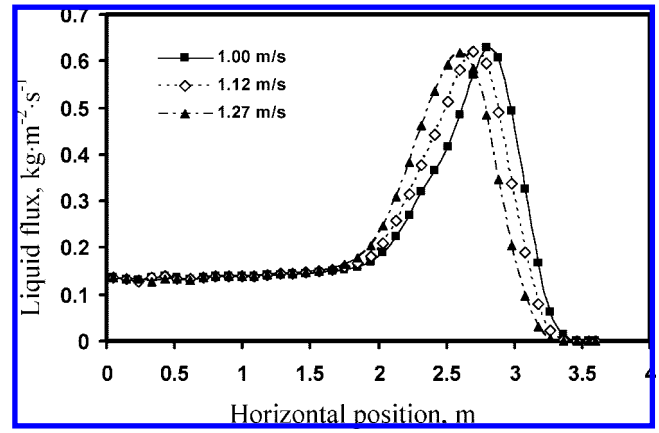

Figure 12. Comparison of the outlet liquid flux at the bottom for different gas flow rates.

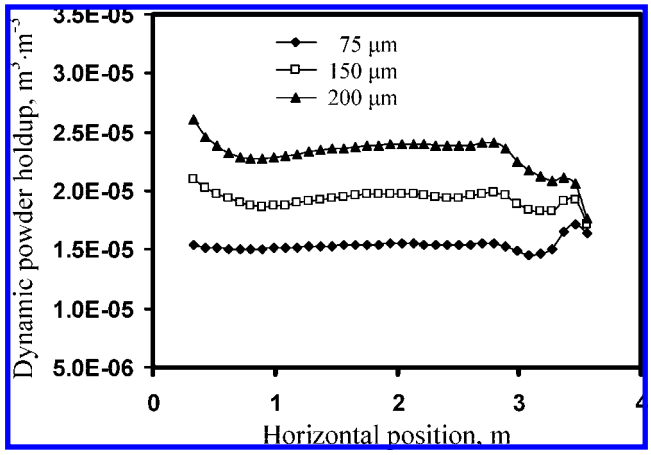

Figure 13. Horizontal dynamic powder holdup distribution at the inlet height for different powder diameters.

deadman decreases (case 2), the dynamic and static liquid holdups increase, as shown in Figure 6b. With powder consumption considered, although there is little change in the general trend of liquid holdup distribution, as shown in Figure 6c, the region of high liquid holdup shrinks with a reduced powder accumulation region in the deadman.

Figures 6 and 7 show the effect of different regional properties on powder holdup. When the particle size in the deadman decreases to 20 mm while remaining constant in the coke zone (30 mm), two large powder holdup regions can be observed close to the surface of the deadman and between the deadman and the CZ. There is a distinct interface between the coke zone and the deadman. It indicates that the dynamic powder holdup is very sensitive to the local mean particle size, which has a significant effect on the gas−powder flow. Similar results were also reported by Yagi et al.,[46] but they were for gas phase flow only. Their results show that the flow pattern of gas is governed by the bed structure. However, little attention was paid to the flow behavior in the lower part of the furnace. The present results also indicate that, above the CZ, plumelike distributions for dynamic powder holdup are predicted, and these are similar to those reported by Ichida et al.[47] Figure 8a shows that a smaller particle size in the deadman can increase the total holdup and, correspondingly, the powder accumulation region in the central lower part of the furnace. This is consistent with the phenomena found by Pinson,[48] i.e., the contact numbers per unit bed volume for particles increase as the particle size decreases, so that powder is entrapped more easily. Similar trends were also observed by Sugiyama[26] in a laboratory scale study, where powder holdup evidently increases in a packed bed with small packed particle size.

Another interesting phenomenon is the effect of porosity distribution on gas−powder flow, as shown in Figures 6b and 7b. When porosity in the deadman decreases, the dynamic powder holdup correspondingly decreases, because of the increase in flow resistance. As reported by Pandey et al.,[49] with a 10% decrease in porosity, the resistance to fluid flow increases by 300%. This results in less powder passing through the deadman. In contrast, because the gas flow rate also decreases with the resistance, a higher static holdup is obtained. The situation is such that the static holdup is higher but the dynamic holdup is lower: the total holdup actually increases in the deadman. This suggests that the change of dynamic powder holdup with the porosity distribution may be inconsistent with that of static powder holdup, especially for the complex BF system.

In practice, it is important for blast furnace operators to understand the consumption behavior of unburnt char. The cases previously discussed ignore the consumption of fine powder in the furnace. After leaving the raceway, the unburnt char may react with or be assimilated by other phases, including gas and slag phases. That is, char may be used in ore reduction and the dissolution of char into the hot metal.

Different consumption rates for char in separate regions have been assumed in case 3, with char or unburnt coal powder assumed to be uniformly consumed in every given region. Figure 7c shows that the maximum dynamic powder holdup is located lower in the furnace at the bottom of the coke zone. This suggests that, when liquids percolate through the coke zone, it is more probable that the liquids interact with unburnt char at the bottom of this zone. The dynamic holdup gradually decreases along the flow direction in the lower part of the furnace. Above the CZ, the powder holdup distributes along the streamlines, because of the low powder consumption rate. Only a small amount of char leaves the furnace. As reported by Yamaguchi et al.,[50] this unburnt char carryover in the off-gas can be used to determine constraints on a furnace with PCI. Figure 8c shows that the total holdup is relatively large in the deadman, because of the lower gas velocity and particle diameter. Similar phenomena were observed by Chen et al.[25] in a gas−powder flow system (i.e., a higher total powder holdup exists in the lower central part of a packed bed where gas has a low velocity).

Figure 9 shows the streamlines of the four phases for case 2. Compared to the previous results (see Figure 3), the difference is minor. However, when gas and powder flow through the deadman, there is a deviation in the flow direction. As described in section 4.1, a strong horizontal gas flow can form between the fused layers, which can cause liquid droplets generated in the fused layer to flow horizontally between the layers (see Figure 9b). As shown in Figure 9a, when burden flows down through the CZ, burden materials soften and melt, leading to the change of flow pattern from the plug flow to converged flow.

4.3. Effect of Operational Conditions. Different operational conditions have also been used in the simulation, including different powder diameters, gas flow rates, and powder combustion rates, using the packing property of case 2.

Figures 10 and 11 show the calculated the dynamic holdup and total holdup of powders in the blast furnace at different superficial gas velocities. They indicate that the powder accumulation region increases as the gas velocity decreases, so that the deadman becomes cleaner (viz., has higher voidage), because of shrinkage of the powder accumulation zone. This phenomenon has been observed in physical experiments with simple geometries.[25,30] Practically, increasing the superficial gas velocity improves chemical reaction rates, interphase heat exchange, and BF productivity. However, a high blast velocity can cause coke fragmentation in front of the tuyeres, which can lead to an accumulation of fines in the deadman and a decrease in bed permeability. Also, the potential for local fluidization should be considered when the gas velocity is increased, as discussed by Castro et al.[51] and Sugiyama.[52]

With an increase of gas flow rate, liquid flow shifts away from the gas inlet. This results in enlargement of the dry zone and denser static holdup in the entire lower portion of the furnace. Liquid flux variation over the furnace bottom cross-section is depicted in Figure 12, where it can be observed that the peak of liquid flux shifts toward the center as the gas flow rate increases. Two regions in which liquid flow is strongly affected by the high horizontal component of gas velocity can

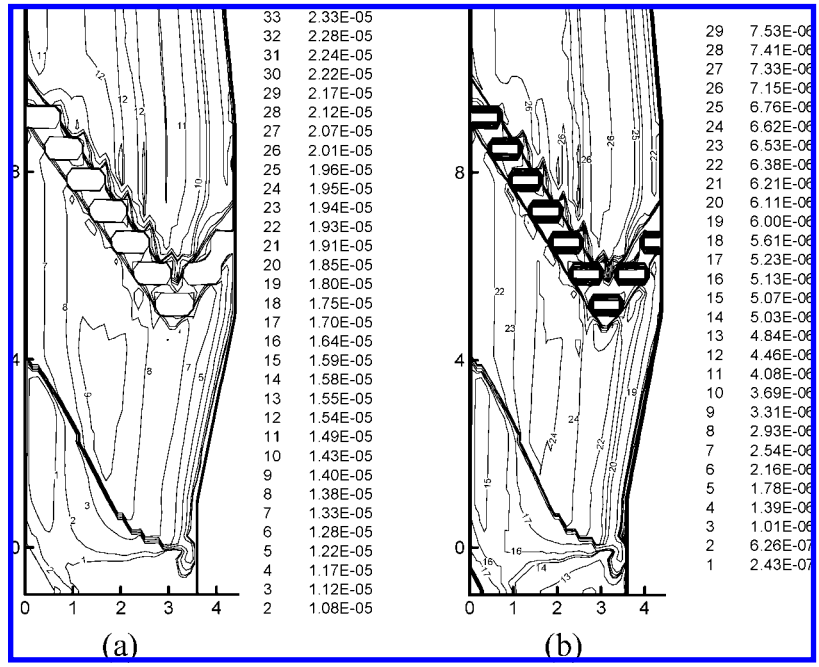

Figure 14. Comparison of dynamic powder holdup for different powder combustion rates in the raceway: (a) 36% and (b) 84%.

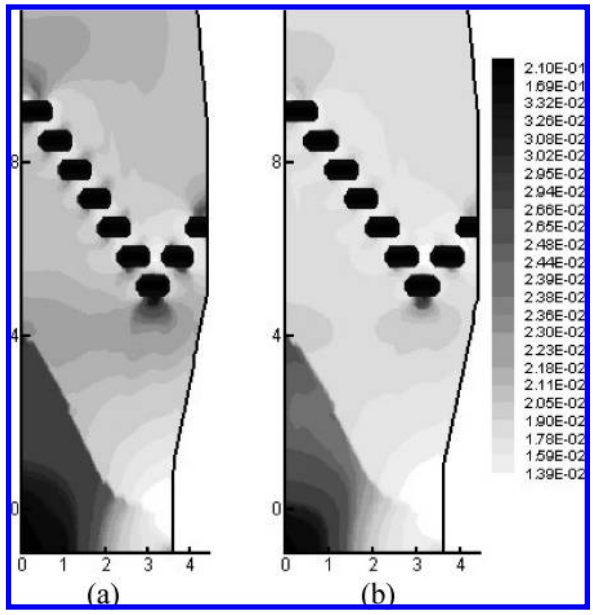

Figure 15. Comparison of total powder holdup for different powder combustion rates in the raceway: (a) 36% and (b) 84%.

be identified: one is between the fused layers, and another is in front of the tuyere. In these two regions, high liquid holdup can form locally, because the pore space in the coke zone may be filled with the liquid that is convected and deposited by the strong gas flow.

In practice, the size of unburned coal particles leaving the raceway is an important factor that affects the permeability in the lower portion of a furnace. Figure 13 shows the distribution of the dynamic holdup at the tuyere level for unburned coal particles of different sizes. The calculation was performed for the injection of mean powder diameters in the range of 75−200 μm. The results indicate that the dynamic powder holdup can increase as the powder diameter increases for a given powder flux. The inlet dynamic holdup is almost the same in all cases. However, at the central part of the furnace, the magnitude of dynamic holdup increases by a factor of 1.5 when the powder diameter changes from 75 μm to 200 μm, which is consistent with the finding by Hidaka et al.,[53] that the dynamic holdup of large powder (220 μm Fine Glass Beads (FGBs)) increased 2-fold over that of fine powder (65 and 118 μm FGBs).

Most of the pulverized coal (PC) that is blown through the tuyeres rapidly burns in the raceway.[54] Some of unburned PC can enter the furnace together with gas, with the combustion efficiency of PC in the raceway directly affecting the amount of unburned PC. Based on the study done by Yamagata et al.,[55] the consumption rate of injected PC in the raceway was assumed to be 36% or 84% for a PCI rate of 250 kg/THM. The calculated results are shown in Figures 13 and 14, suggesting that the powder accumulation region significantly decreases and dynamic holdup becomes more lower when the coal combustion rate increases to 84%. Figure 15 shows that the affected region is the deadman and the lowest part of CZ. This indicates that if the combustion rate decreases, the permeability of these two regions is predicted to deteriorate.

4.4. Role of Powder−Liquid Interaction. In the theoretical formulation, the interactions between phases are taken into account, in terms of the volume fraction and interaction forces. However, in the aforementioned sections, the interaction between powder and liquid is only presented by the volume fraction. The correlation for powder−liquid interaction force is not available yet, although some experimental studies have been conducted in this direction.[43,48,56] The liquid−powder interaction force was ignored in the previous mathematical models.[14,38] As part of this work to examine the effectiveness of this treatment, a presumed powder−liquid interaction force is proposed by the following equation, similar to the powder−solid interaction force:

$$\mathbf{F}_{\mathrm{f}}^{l} = -\frac{1}{2d_l}\rho_{\mathrm{f}}\varepsilon_{\mathrm{fd}}|\mathbf{u}_{\mathrm{f}} - \mathbf{u}_l|f_l(\mathbf{u}_{\mathrm{f}} - \mathbf{u}_l) \tag{9}$$

where f_l is treated as a function of liquid Froude number ($f_l = 14.98/Fr_l^{1.33}$).

A sensitivity analysis has been performed by adding this force into the momentum equation of the powder phase. Three cases are considered with different magnitudes of this interaction

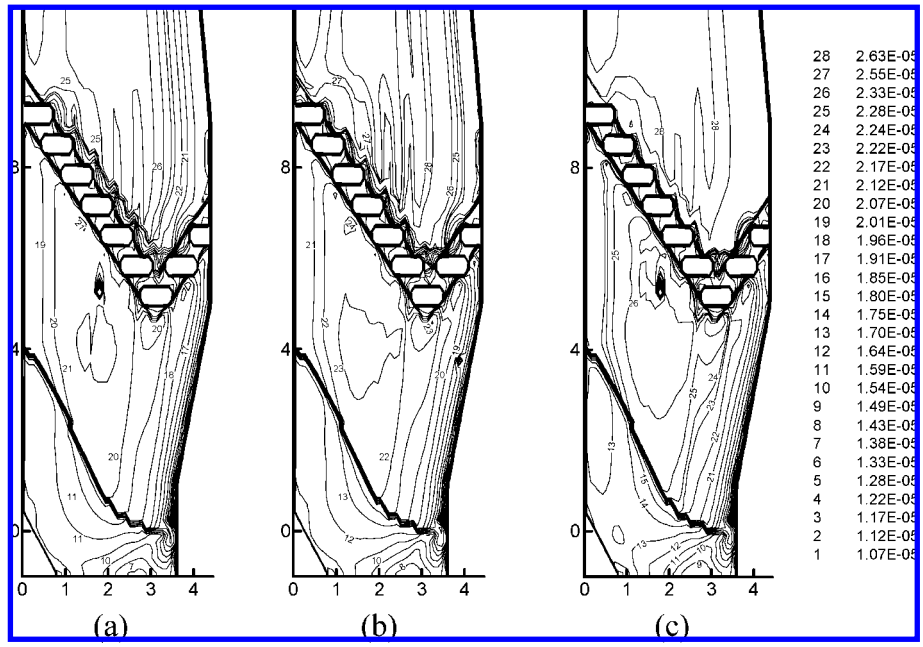

Figure 16. Effect of F_f^l on the dynamic powder holdup for case 3: (a) $0.5F_f^l$, (b) F_f^l, and (c) $1.5F_f^l$.

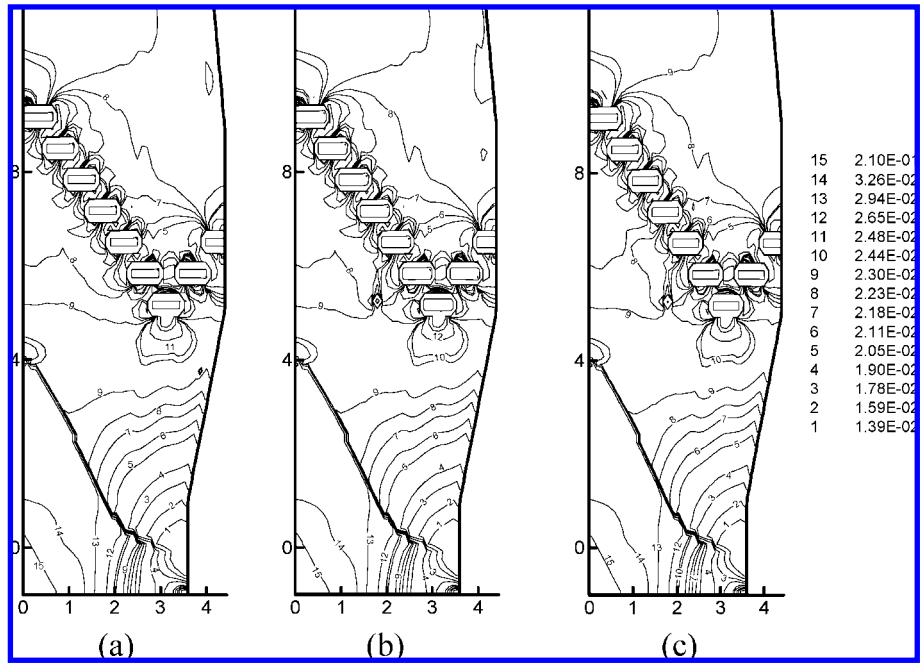

Figure 17. Effect of F_f^l on the total powder holdup for case 3: (a) $0.5F_f^l$, (b) F_f^l, and (c) $1.5F_f^l$.

force, i.e., $0.5F_f^l$, F_f^l, and $1.5F_f^l$. Figure 16 shows the effect of F_f^l on the dynamic powder holdup distribution. The dynamic powder holdup in the lower portion of the BF increases when F_f^l is considered in the simulation. In particular, the magnitude of the dynamic powder holdup increases as F_f^l increases. The total powder holdup also slightly increases as shown in Figure 17. However, the results suggest that the overall powder flow pattern is not affected much by F_f^l. They have offered a reason why this force can be ignored in the previous studies.[14,38] However, note that the present presumed interaction force only considers the collision and friction between powders and liquid droplets with similarity toF_f^s. Some fundamental properties of the liquid phase have not been taken into account in the present work, such as liquid−powder wetting. Therefore, more detailed work in this direction should be undertaken in the future.

5. Conclusions

A mathematical model has been proposed to describe the gas−powder−liquid−solid four-phase flow in a blast furnace (BF). The model is shown to be able to capture the in-furnace key flow patterns that have been established in the literature. The model results demonstrate the following:

(1) A layered cohesive zone induces a strong horizontal gas−powder flow in the coke slits, a stratified distribution of dynamic powder holdup in the shaft, and a strong maldistribution of liquid holdup in the lower part of BF, which should not be ignored in BF simulations.

(2) The motion and structure of solids have a significant effect on powder and liquid holdup distributions. A region such as a solid stagnant zone with small coke particles and low porosity

is likely to hold more liquid and powder, resulting in low permeability.

(3) Powder holdup intends to increase with increasing powder size or decreasing gas flow rate. However, it changes significantly when powder consumption is considered. A high combustion rate of injected pulverized coal can reduce the powder accumulation region greatly.

(4) It is likely that fluid flow pattern does not change much with the inclusion of the interaction force between powder and liquid. However, further investigation is needed to verify this treatment, particularly for conditions of different fluid properties.

Finally, note that, to predict and optimize BF performance, the fluid flow model must be coupled with heat-transfer and chemical reactions and consider the phase properties, which vary with temperature and components. The flow model described in this work provides a sound basis to achieve this goal.

Nomenclature

A_{ij} = effective contact area between phases i and j in unit volume of bed (m^2/m^3)
c_1 = empirical coefficient
CCR = coal consumption rate (kg tHM^{-1})
Cd = empirical coefficient for drag force
Cp_m = modified liquid Capiliary number; $Cp_m = \rho_l g \varphi^2 d_p^2/\sigma(1 - \varepsilon)^2(1 + \cos\theta)$
CSO = coke solution in the dripping zone and deadman (kg tHM^{-1})
d = diameter (m)
$d_{l,g}$ = liquid droplet diameter, as affected by gas flow (m)
$d_{l,h}$ = droplet diameter, as affected by holdup (m)
d_w = effective packing diameter (m)
D^* = hydrodynamic equivalent diameter; $D^* = 2\varphi_s d_s(1 - \varepsilon_s)/3\varepsilon_s$ (m)
f_l, f_k = coefficients
$\mathbf{F}$ = interaction force per unit volume (kg m^{-2} s^{-2})
Fr_i = Froude number; $Fr_i = u_i(D^*g)^{-0.5}$
g = magnitude of gravitational acceleration; $g = 9.81$ m/s^2
$\mathbf{g}$ = gravitational acceleration (m/s^2)
G = mass flow rate (kg m^{-2} s^{-1})
h = holdup
h_{lt} = total holdup
h_{lt0} = total holdup without gas flow
$\mathbf{I}$ = identity tensor
OSM = pore shrinkage and meltdown in the cohesive zone (kg tHM^{-1})
p = pressure (Pa)
$\Delta P_e/\Delta x$ = effective pressure gradient (Pa/m)
Re_i = Reynolds number; $Re_{tg} = \rho_g U_g d_s/\mu_g$ and $Re_f = \phi_f d_f \rho_g \varepsilon_g |\mathbf{u}_g - \mathbf{u}_f|/\mu_g$
S = source term
$S_{flow\ rate}$ = burden flow rate (kg/s)
$S_{hot\ metal}$ = productivity (kg/s)
TCO = total ore and coke consumption in the furnace (kg tHM^{-1})
$\mathbf{u}$ = interstitial velocity (m/s)
U = superficial velocity (m/s)
$\mathbf{U}$ = superficial velocity vector (m/s)
VOL = zone volume (m^3)
x = spatial coordinate (m)
X_p = dimensionless pressure drop

Greek Symbols

α, β = incline angles
α_l = relaxation factor
ε = volume fraction
θ = contact angle (°)
λ_f = mean distance between particles (m)
μ = viscosity (kg m^{-1} s^{-1})
ρ = density (kg/m^3)
σ = surface tension (N/m)
$\boldsymbol{\tau}$ = stress tensor (Pa)
φ = shape factor
Ψ = general variable

Subscripts

bcz = below the cohesive zone
cz = cohesive zone
ld = dynamic liquid
f = powder
fd = dynamic powder
fs = static powder
F = fixed bed
g = gas
i = identifier (g, f, or s)
l = liquid
ls = static liquid
M = moving bed
s = solid
t = total
w = wall

Superscripts

n_1, n_2 = empirical coefficients
g = gas
ld = dynamic liquid
max = maximum
T = transpose
fd = dynamic powder
s = solid

Acknowledgment

The authors are grateful to the Australian Research Council and BlueScope Steel for the financial support of this work. The authors are grateful to Dr. P. Austin, Dr. B. Wright, Dr. D. Maldonado, and Dr. B. Guo for helpful discussion.

Literature Cited

(1) Burgess, J. Ironmaking—an overview. *Aust. Coal J.* **1993**, *42*, 29–35.

(2) Yagi, J. Mathematical modelling of the flow of four fluids in a packed bed. *ISIJ Int.* **1993**, *33*, 619–639.

(3) Dong, X. F.; Yu, A. B.; Yagi, J.; Zulli, P. Modelling of multiphase flow in a blast furnace: recent developments and future work. *ISIJ Int.* **2007**, *47*, 1553–1570.

(4) Cundall, P. A.; Strack, O. D. L. A discrete numerical model for granular assemblies. *Geotechnique* **1979**, *29*, 47–65.

(5) Wright, B. D. Formation of stagnant zones during discrete particle simulations of flowing solids; BHP Research and Technology Development Note, Wollongong, Australia, June 29, 1998, No. N98/021.

(6) Nedderman, R. M.; Tüzün, U. Kinematic model for the flow of granular-materials. *Powder Technol.* **1979**, *22*, 243–253.

(7) Takahashi, H.; Kushima, K.; Takeuchi, T. Two dimensional analysis of burden flow in blast furnace based on plasticity theory. *ISIJ Int.* **1989**, *29*, 117–124.

(8) Takahashi, H.; Komatsu, N. Cold model study on burden behaviour in the lower part of blast furnace. *ISIJ Int.* **1993**, *33*, 655–663.

(9) Chen, J.; Akiyama, T.; Nogami, H.; Yagi, J.; Takahashi, H. Modeling of solid flow in moving beds. *ISIJ Int.* **1993**, *33*, 664–671.

(10) Zhang, S. J.; Yu, A. B.; Zulli, P.; Wright, B.; Tuzun, U. Modelling of the solids flow in a blast furnace. *ISIJ Int.* **1998**, *38*, 1311–1319.

(11) Zaïmi, S. A.; Akiyama, T.; Guillot, J. B.; Yagi, J. Validation of a blast furnace solid flow model using reliable 3-D experimental results. *ISIJ Int.* **2000**, *40*, 332–341.

(12) Szekely, J.; Kajiwara, Y. Mathematical representation of spatially non-uniform, counter-current flow of gases and liquids in packed beds of

relevance to flow phenomena in the bosh of iron blast furnaces. *ISIJ Int.* **1979**, *19*, 76–84.

(13) Sugiyama, T.; Sugata, M. Development of two-dimensional mathematical model for the blast-furnace; Nippon Steel Technical Report No. 35, October 1987, pp 32−42.

(14) Austin, P. R. Modelling of the Blast Furnace Based on the Multifluid Concept with Applications to Advanced Operations, Ph.D. Thesis, Tohoku University, Japan, 1997.

(15) Ohno, Y.; Schneider, M. Effect of horizontal gas flow on liquid dropping flow in two-dimensional packed bed. *Tetsu-to-Hagane* **1988**, *74*, 923–1930.

(16) Wang, J.; Takahashi, R.; Yagi, J. Simulation model of the gas-liquid flows in the packed bed. *Tetsu-to-Hagane* **1991**, *77*, 1585–1592.

(17) Eto, Y.; Takeda, K.; Miyagawa, S.; Taguchi, S.; Itaya, H. Experiments and simulation of the liquid flow in the dropping zone of a blast furnace. *ISIJ Int.* **1993**, *33*, 681–686.

(18) Gupta, G. S.; Litster, J. D.; Rudolph, V. R.; White, E. T.; Domanti, A. Model studies of liquid flow in the blast furnace lower zone. *ISIJ Int.* **1996**, *36*, 32–39.

(19) Wang, G. X.; Chew, S. J.; Yu, A. B.; Zulli, P. Modeling the discontinuous liquid flow in a blast furnace. *Metall. Mater. Trans. B* **1997**, *28B*, 333–343.

(20) Chew, S. J.; Zulli, P.; Yu, A. B. Modelling of liquid flow in the blast furnace: theoretical analysis of the effects of gas, liquid and packing properties. *ISIJ Int.* **2001**, *41*, 1112–1121.

(21) Chew, S. J.; Zulli, P.; Yu, A. B. Modelling of liquid flow in the blast furnace: application in a comprehensive blast furnace model. *ISIJ Int.* **2001**, *41*, 1122–1130.

(22) Wang, G. X.; Litster, J.; Yu, A. B. Simulation of gas-liquid flow in dripping zone of blast furnace involving impermeable fused layers. *ISIJ Int.* **2000**, *40*, 627–636.

(23) Yamaoka, H. Flow characteristics of gas and fine particles in a two-dimensional space of packed bed. *Tetsu-to-Hagane* **1986**, *72*, 2194–2201.

(24) Shibata, K.; Shimizu, M.; Inaba, S.; Takahashi, R.; Yagi, J. Pressure loss and hold up powders for gas-powder two phase flow in packed beds. *ISIJ Int.* **1991**, *31*, 434–439.

(25) Chen, J.; Akiyama, T.; Nogami, H.; Yagi, J. Behavior of powders in a packed bed with lateral inlets. *ISIJ Int.* **1994**, *34*, 133–139.

(26) Sugiyama, T. Analysis on the powder movement and accumulation in the deadman and dripping zone of blast furnace by the experiment of the powder−gas 2-phase flow through the parallel packed bed. *CAMP−ISIJ* **1996**, *9*, 19–21.

(27) Hidaka, N.; Matsumoto, T.; Kusakabe, K.; Morooka, S. Transient accumulation behavior of fines in packed beds of pulverized coke particles. *J. Chem. Eng. Jpn.* **2000**, *33*, 152–159.

(28) Pintowantoro, S.; Nogami, H.; Yagi, J. Numerical analysis of static holdup of fine particles in blast furnace. *ISIJ Int.* **2004**, *44*, 304–309.

(29) Nogami, H.; Austin, P. R.; Yagi, J.; Yamaguchi, K. Numerical investigation on effects of deadman structure and powder properties on gas and powder flows in lower part of blast furnace. *ISIJ Int.* **2004**, *44*, 500–509.

(30) Dong, X. F.; Pinson, D.; Zhang, S. J.; Yu, A. B.; Zulli, P. Gas-powder flow and powder accumulation in a packed bed. I: Experimental study. *Powder Technol.* **2004**, *149*, 1–9.

(31) Dong, X. F.; Zhang, S. J.; Pinson, D.; Yu, A. B.; Zulli, P. Gas-powder flow and powder accumulation in a packed bed. II: Numerical study. *Powder Technol.* **2004**, *149*, 10–22.

(32) Yuu, S.; Umekage, T.; Miyahara, T. Predicition of stable and unstable flows in blast furnace raceway using numerical simulation methods for gas and particles. *ISIJ Int.* **2005**, *45*, 1406–1415.

(33) Takeda, K.; Lockwood, F. C. Stochastic model of flow and dispersion of fine particles in a packed bed. *Tetsu-to-Hagane* **1996**, *82*, 492–497.

(34) Takeda, K.; Lockwood, F. C. Integrated mathematical model of pulverised coal combustion in a blast furnace. *ISIJ Int.* **1997**, *37*, 432–440.

(35) Dong, X. F.; Pinson, D.; Zhang, S. J.; Yu, A. B.; Zulli, P. Gas−powder flow in blast furnace with different shapes of cohesive zone. *Appl. Math. Modell.* **2006**, *30*, 1293–1309.

(36) Kuwabara, M.; Takane, S.; Sekido, K.; Muchi, I. Mathmatical two-dimensional model of the blast furnace process. *Tetsu-to-Hagane* **1991**, *77*, 1593–1600.

(37) Takatani, K.; Inada, T.; Ujisawa, Y. 3-dimensional dynamic mathematical simulator of blast furnace. *CAMP−ISIJ* **1994**, *7*, 50–53.

(38) Castro, J.; Nogami, H.; Yagi, J. Transient mathematical model of blast furnace based on multi-fluid concept with application to high PCI operation. *ISIJ Int.* **2000**, *40*, 637–646.

(39) Gidaspow, D.; Ettehadieh, B. Fluidization in two-dimensional beds with a jet. 2. Hydrodynamic modelling. *Ind. Eng. Chem. Fundam.* **1983**, *22*, 193–201.

(40) Eldighidy, S. M.; Chen, R. Y.; Comparin, R. A. Deposition of suspensions in the entrance of a channel. *J. Fluids Eng.−Trans. ASME* **1977**, *99*, 365–370.

(41) Zhang, S. J.; Yu, A. B.; Zulli, P.; Wright, B.; Austin, P. Numerical simulation of solids flow in a blast furnace. *Appl. Math. Modell.* **2002**, *26*, 141–154.

(42) Yu, A. B.; Standish, N. Estimation of the porosity of particle mixtures by a linear-mixture packing model. *Ind. Eng. Chem. Res.* **1991**, *30*, 1372–1385.

(43) Pham, T. Gas-powder-liquid three-fluid flow in moving particles for blast furnace modelling, Ph.D. Thesis, University of New South Wales, Sydney, Australia, 2001.

(44) Omori, Y. *Blast Furnace Phenomena and Modelling*; Elsevier Applied Science: London, 1987.

(45) Chew, S. J.; Wang, G. X.; Yu, A. B.; Zulli, P. Experimental study of liquid flow in blast furnace cohesive zone. *Ironmaking Steelmaking* **1997**, *24*, 392–400.

(46) Yagi, J.; Takeda, K.; Omori, Y. Two-dimensional simulation on the gas flow and heat transfer in the blast furnace. *ISIJ Int.* **1982**, *22*, 884–892.

(47) Ichida, M.; Nakayama, T.; Tamura, K.; Shiota, H.; Araki, K.; Sugisaki, Y. Behavior of fines in the blast furnace. *ISIJ Int.* **1992**, *32*, 505–513.

(48) Pinson, D. Gas, powder and liquid flow in packed bed, Ph.D. Thesis, University of New South Wales, Sydney, Australia, 1998.

(49) Pandey, B. D.; Yadav, U. S. Blast furnace performance as influenced by burden distribution. *Ironmaking Steelmaking* **1999**, *26*, 187–192.

(50) Yamaguchi, K.; Ueno, H.; Tamura, K. Maximum injection rate of pulverized coal into blast furnace through tuyeres with consideration of unburnt char. *ISIJ Int.* **1992**, *32*, 716–724.

(51) Castro, J.; Nogami, H.; Yagi, J. Numerical investigation of simultaneous injection of pulverized coal and natural gas with oxygen enrichment to the blast furnace. *ISIJ Int.* **2002**, *42*, 1203–1211.

(52) Sugiyama, T. Numerical simulation for stable operation factors under the high PC ratio. In *International Blast Furnace Lower Zone Symposium*, Wollongong, Australia, November 25−27, 2002; pp 131−136..

(53) Hidaka, N.; Iyama, J.; Matsumoto, T.; Kusakabe, K.; Morooka, S. Entrainment of fine particles with upward gas flow in a packed bed of coarse particles. *Powder Technol.* **1998**, *95*, 265–271.

(54) Iwanaga, Y. Investigation on behavior of unburnt pulverized coal in blast furnace. *ISIJ Int.* **1991**, *31*, 494–499.

(55) Yamagata, C.; Suyama, S.; Horisaka, S.; Takatani, K.; Kajiwara, Y.; Komatsu, S.; Shibuta, H.; Aminaga, Y. Fundamental study on combustion of pulverized coal injected into coke bed at high rate. *ISIJ Int.* **1992**, *32*, 725–732.

(56) Horio, M. Powder accumulation characteristics in two-dimensional packed fluidised bed. Report of Committee on Transport Phenomena in Gas−Solid−Liquid Packed Bed, ISIJ, Section 2.4, 1993, pp 1−23.

Received for review January 26, 2008
Revised manuscript received April 20, 2008
Accepted April 28, 2008

IE800147V